PROCEEDINGS
OF
THE ELEVENTH INTERNATIONAL SYMPOSIUM
ON
SPACE TECHNOLOGY
AND
SCIENCE

TOKYO
1975

Influence of a Reradiative Heating Constraint on Lifting Entry Trajectories for Maximum Lateral Range*

Ernst D. DICKMANNS** and Hans-J. PESCH***

Abstract

A precise numerical optimization algorithm (multiple shooting) is used to investigate the heating constrained crossrange maximization problem for a Space Shuttle orbiter-type vehicle. The effect of limit skin temperature is discussed in detail. One to four constrained arcs were encountered for a relatively steep entry angle. The constraint is shown to smooth out the oscillatory behaviour typically encountered with entry conditions not corresponding to quasisteady glide.

1. Introduction

With the advent of the Space Shuttle atmospheric entry with lifting vehicles capable of considerable lateral ranging will become of practical interest. The lateral range capacity will allow increased return frequencies from orbit to given landing sites. Though the practical problem for later operations will be the spot-landing within the range footprint while minimizing some other payoff-function (e.g. some heating indicator) for general mission analysis the maximally achievable lateral range is of prime interest. This problem has been treated in (Ref. 1). There a simple analytical approximate solution has been given for vehicles entering under a small flight path angle from close satellite orbits and having lift to drag ratios $L/D \simeq \pi/2$. Comparisons with numerically computed optimal trajectories showed good agreement; typical oscillating trajectories for entry conditions not corresponding to quasisteady glide (QSG) could be duplicated by a superposition of the QSG-solution and those resulting from a linearized set of equations developed around the QSG-solution; this may be utilized for the development of a guidance algorithm.

In addition numerical results for maximum lateral range taking a velocity-, altitude-, and angle of attack-dependant heating constraint into account were given. Those results were obtained with a gradient method and the iterations were stopped rather early when the range gain per iteration became small.

Purpose of this paper is to present more accurate numerical solutions obtained in the meantime (Ref. 2) utilizing a multiple shooting algorithm due to Bulirsch (Ref. 3) and Deuflhard (4, 5). This algorithm allows solutions of illconditioned problems to a degree of exactness which is hardly achievable by gradient or parameterization methods in wide use today.

---

*This research was supported by Professor Dr. Roland Bulirsch, Mathematisches Institut, Universität Köln, FRG, by providing the optimization algorithm and the computer time.

**Dr.-Ing., Institut für Dynamik der Flugsysteme, Deutsche Forschungs- und Versuchsanstalt für Luft- und Raumfahrt E.V., Oberpfaffenhofen, Bavaria, Federal Republic of Germany.

***Dipl.-Math., Institut für Mathematik, Technische Universität München, Bavaria, Federal Republic of Germany.

2. Coordinate System

The equations of motion are written in a flight path oriented axis system, the x-axis of which is aligned with the velocity vector. The z-axis is downward in the vertical plane, and the origin of this right-handed system is based in the vehicle center of gravity (c.g.). The position of the vehicle c.g. with respect to the planet is specified by the downrange angle Θ, the cross-range angle Λ and the radial distance $r = R + h$ (Fig. 1). The heading angle relative to the initial conditions is designated by χ, positive for right turns.

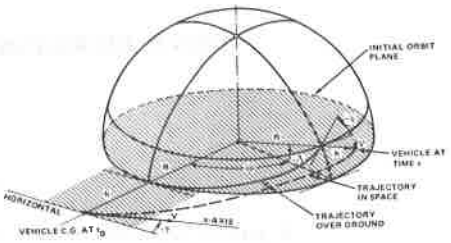

Figure 1. Coordinate system.

3. Mathematical Model

Assumptions to arrive at a relatively simple mathematical model are discussed in (Ref. 1): assuming no planet rotation and oblatenes, no winds and a stationary atmosphere, a point mass vehicle and a constant drag polar the equations of motion in a flight path oriented coordinate system may be written (general form $\dot{x} = f(x,u)$; $u^T = (C_L, \mu)$):

$$\dot{V} = -g \sin\gamma - \frac{D}{m}$$

$$\dot{\chi} = -\frac{V}{r} \cos\gamma \cos\chi \tan\Lambda + \frac{L}{Vm} \frac{\sin\mu}{\cos\gamma}$$

$$\dot{\gamma} = \left(\frac{V}{r} - \frac{g}{V}\right)\cos\gamma + \frac{L}{Vm} \cos\mu \qquad (1)$$

$$\dot{\Theta} = \frac{V}{r} \frac{\cos\gamma}{\cos\Lambda} \cos\chi$$

$$\dot{\Lambda} = \frac{V}{r} \cos\gamma \sin\chi$$

$$\dot{r} = \dot{h} = V \sin\gamma$$

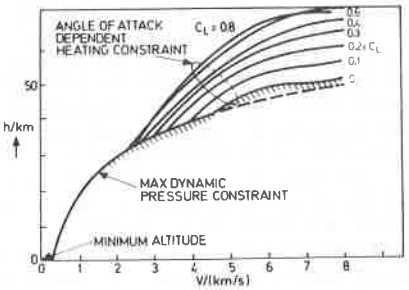

2a. Qualitative altitude constraints for reentry.

where

$$\begin{bmatrix} L \\ D \end{bmatrix} = \begin{bmatrix} C_L \\ C_D \end{bmatrix} S \frac{\rho}{2} V^2 \qquad \begin{matrix} \text{lift} \\ \text{drag} \end{matrix}$$

$$C_D = C_{Do} + k\, C_L^n \qquad \text{drag polar} \qquad (2)$$

$$r = R_o + h \qquad \text{radius vector}$$

$$g = g_o R_o^2/(R_o + h)^2 \qquad \text{gravity acceleration}$$

The allowed state space for the reentering vehicle is constrained to avoid excessive kinetic heating as given in (Ref. 1) (see Fig. 2).

The reradiative heating constraint under these assumptions has the form

$$C = C_L - C_{LH}(V,h) \leq 0 \qquad (3)$$

with C_{LH} given by vehicle data. This is a zeroth order state space

constraint where on the constraint the control C_L is given as a function of altitude and velocity.

The differential equations for the Lagrangian multipliers are rather lengthy and not reproduced here. The interested reader is refered to (Ref. 1). The optimal controls are given by

$$\mu_{opt} = \tan^{-1}[\lambda_\chi/(\lambda_\gamma \cos\gamma)] \tag{4}$$

and

$$C_{Lopt} = \left[\frac{w}{V\ \lambda_V\ k\ n}\right]^{1/(n-1)} \quad \text{on unconstrained arcs} \tag{5}$$

where

$$w = -\left[(\lambda_\chi/\cos\gamma)^2 + \lambda_\gamma^2\right]^{1/2} . \tag{6}$$

On constrained arcs there appear additive terms in the adjoint differential equations.

For a Space Shuttle-orbiter-type vehicle the following characteristics have been assumed:

$$C_{Do} = 0.04\ ;\quad k = 1.0\ ;\quad n = 1.86 \text{ and } \frac{m}{S} = 250[kg/m^2]$$

resulting in a maximum inverse glide number of

$$E = (C_L/C_D)_{max} = 2.22 \quad \text{at} \quad C_{LE} = 0.192 . \tag{7}$$

4. Numerical Method

The numerical results presented below have been obtained by taking advantage of the existence of a comparatively accurate optimization algorithm due to Bulirsch (Ref. 3) and Deuflhard (Ref. 4, 5). It had been developed on the basis of the known multiple shooting scheme and especially trimmed to handle almost singular problems as the one considered here.

Numerical results in (Ref. 1) had been obtained with a min-H procedure (a refined gradient algorithm) and can only be considered as relatively crude approximations since the iteration had been stopped when the performance gain per iteration became small. The numerically accurate optimal controls may still deviate considerably from the ones obtained though the payoff function is close to the extremum.

The difficulties which had to be overcome to obtain the results given below using the multiple shooting method are described in (Ref. 2). The condition number of the iteration matrix went up to 10^{19} for the solution with $\Delta C_{AH} = 0.008$. The effort to obtain these results was large (for routine investigations may be prohibitive) but it may be very hard to obtain them at all to this degree of accuracy using other numerical methods. A different formulation leading to more well conditioned behaviour is needed.

5. Discussion of Results

First the *unconstrained footprint maximization* for the vehicle and boundary conditions specified above will be discussed: Fig. 3a and b show the time history of the controls bank angle μ and lift coefficient C_L for different footprint parameters p. In Fig. 3c the corresponding ground tracks and the footprint envelope is given. For p = 0 the lift coefficient is almost constant at $C_L = C_{LE}$ and the bank angle has an almost constant decrease rate (after an initial constant bank angle while the vehicle is above the QSG-altitude) as indicated by the *basic* solution derived in (Ref. 1). The decrease rate, however, is about 12% higher than indicated by the simple relation in the non-dimensionalized variables $d\mu/d\tau \simeq -D/L$. Arcs with the same constant bank angle rate appear for values of p up to about 0.5; for increasing p these arcs are preceded by trajectory portions with positive bank angle rates where μ starts from decreasing bank angle values (Fig. 3a;

compare also results given in (Ref. 1) for L/D = 1.4 (Fig.10)). It is seen that as soon as downrange angles of π are reached the initial bank angle $\mu(t_o)$ is slightly negative, which is reasonable from physical considerations. For increasing p the lift coefficient assumes a more pronounced oscillatory behaviour to reduce the altitude oscillations induced by the non-QSG entry flight path angle (Ref. 1). For p = 0 the first skip in altitude is from $h_{min} \simeq 53$ km to about 65 km while for p = 1 it is from $h_{min} = 67$ km to 100 km despite the large reduction in lift coefficient during the first dip (Fig. 3b).

The following discussion is confined to the case *maximum cross range* (p = 0) *with* different levels of *reradiative heating constraints*, i.e. skin temperatures indicated by the parameter ΔC_{AH}. Values of ΔC_{AH} of 0.06, 0.03, 0.008 correspond to limit temperatures of approximately 2400, 2200 and 2050 °F.

Fig. 4 shows a sequence of lift coefficient time histories with various numbers of constrained arcs. Each graph contains two curves: a solid one, the active control, and a dashed one, which on unconstrained arcs represents the heating limit and on constraint arcs the control determined by the maximum principle. Fig. 4a shows the heating constraint violations for $\Delta C_{AH} = 0$ in the entirely unconstrained case. There are two separated violations during the first two dips and a long violation period during the following three.

In the remaining nine graphs of Fig. 4 the heating boundary is moved in: Up to $\Delta C_{AH} = 0.072$ there is only one constrained arc during the first dip. Then three constrained arcs occur (Fig. 4c) followed by a short parameter range with four (Fig. 4d). By decreasing ΔC_{AH} to 0.045 the last two constrained arcs merge together (Fig. 4d and 4e). At $\Delta C_{AH} = 0.035$ the last three arcs have become one of more than 12 min. duration (Fig. 4g). Upon further decreasing ΔC_{AH} the unconstrained arc between the remaining two constrained ones becomes shorter and shorter until at $\Delta C_{AH} = 0.008$ there is only one constrained arc of about 23 minutes left out of about 40 minutes total flight time. The lift coefficient after leaving the constraint is always almost constant at C_{LE}. For lower values of ΔC_{AH} no iterations were tried since the condition number of the iteration matrix had risen from 10^9 at $\Delta C_{AH} = 0.072$ to 10^{19} at $\Delta C_{AH} = 0.008$; this exhausted the double precision word length on the computer used.

Fig. 5 shows a comparison of control time histories for constrained and unconstrained trajectories. With increasing severeness of the constraint (decreasing ΔC_{AH}) the initial bank angle decreases to increase the vertical decelerating component of the lift; this leads to a smooth entry onto a nonoscillating glide arc along the heating constraint for $\Delta C_{AH} = 0.008$ (Fig. 6c). During the first altitude minimum the bank angle increases rapidly to prevent the vehicle from skipping upward too much (Fig. 5a). On the constrained arc the bank angle decreases faster than in the unconstrained case leading to a decrease in heading change at the end of this arc (Fig. 6b,e); this is compensated by a second bank angle increase before leaving the constrained arc which, in conjunction with the lift coefficient program (Fig. 5b) results in an oscillating flight after the heating region is left (Fig. 6c,d and 5c for t > 1600 sec). The smoothing effect of the heating constraint on the trajectory can easily be seen from the load factor curve (Fig. 5c) and the flight path angle and altitude history (Fig. 6c,d, solid line).

The flight time is slightly increased (84 sec $\triangleq$ 3.5%) for the constrained case to reach the same final altitude of 30 km. Downrange increased by 8% while the crossrange decreased by 1.5% (Fig. 6e). The effect of the heating constraint on the costate (adjoint) variables λ_V, λ_χ and λ_Λ is relatively slight (Fig. 6a and 6f). Interesting to note is the fact that the relation derived in (Ref. 1): $\lambda_\chi^2 + \lambda_\Lambda^2 = 1$ is a good approximation in both the unconstrained and the constrained case (insert in Fig. 6f). Strongly influenced by the constraint are the costate variables to the flight path angle and altitude λ_γ and λ_h (Fig. 6g). Before and on the constrained arc large deviations occur. Since λ_χ changes only slightly it is λ_γ that essentially determines

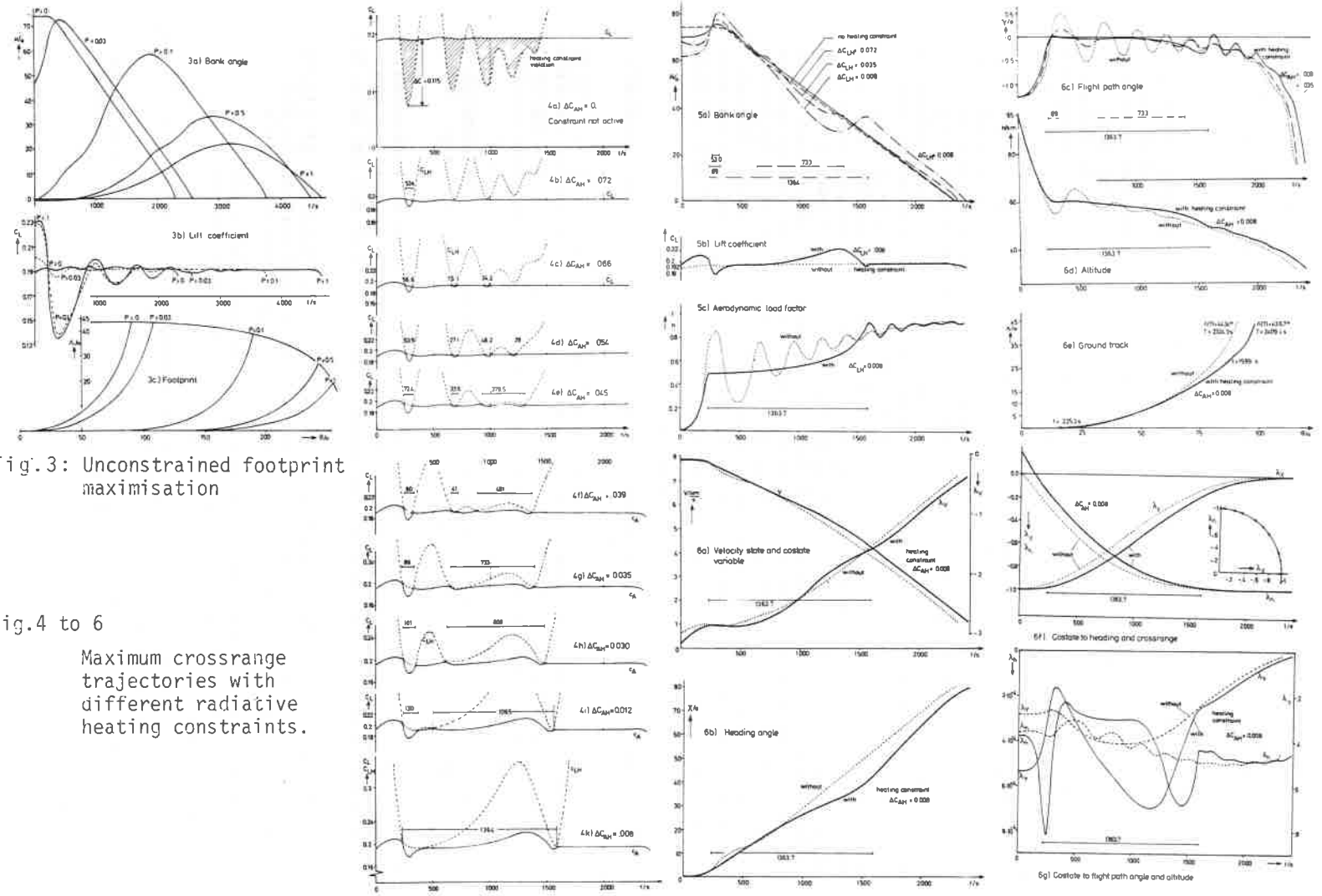

Fig.3: Unconstrained footprint maximisation

Fig.4 to 6

Maximum crossrange trajectories with different radiative heating constraints.

the change in the bank angle control (see eq. (4)). For the unconstrained case and $t > 300$ sec λ_γ has the shape as predicted by the analytical approximate solution in (Ref. 1) ($\nu = \lambda_e D/(L v\sqrt{1-v})$).

6. Conclusion

Precise numerical results for maximum range lifting entry taking a reradiative heating constraint into account were given. Total convective heat transfer and possible trim constraints have not been considered. Under these conditions maximum range trajectories have to be flown with lift coefficients in the close vicinity of the value C_{LE} for best gliding. Bank angle is the prime control both for footprint maximization and skin temperature limitation. Footprint trajectories with large crossranges (over a downrange spectrum of more than 100^o have large portions with approximately constant bank angle rates as predicted by the *basic* solution given in (Ref. 1). If downrange angles in the vicinity of π occur, the bank angle is negative initially.

The assumed heating constraint tends to smooth out trajectory oscillations which are induced by entry conditions not corresponding to quasisteady glide. Depending on the severeness of the heating constraint, one to four constrained arcs occurred. The coolest trajectory achieved ($\simeq 2050\ ^oF$) had one smooth arc of 23 minutes on the constraint and left it with conditions leading to oscillatory behaviour on the adjoining unconstrained arc. Despite the strong reduction in maximum temperature of over 600 degrees F the cross range was decreased by only 1.5%. These trajectories are very sensitive and the condition number of the iteration matrix went up to 10^{19}. For routine calculations a different formulation seems desirable. Multiple shooting, though sometimes not easy to handle proved to be a valuable tool for obtaining precise numerical results even in almost singular problem settings.

References

1. Dickmanns, E.D.: Maximum Range Threedimensional Lifting Planetary Entry. NASA TR R-387 (1972).
2. Pesch, H.J.: Numerische Berechnung optimaler Steuerungen mit Hilfe der Mehrzielmethode, dokumentiert am Problem der optimalen Rückführung eines Raumgleiters unter Berücksichtigung von Aufheizungsbegrenzungen. Diplomarbeit, Mathematisches Institut der Universität Köln (1973).
3. Stoer, J.; Bulirsch, R.: Einführung in die numerische Mathematik II. Springer Verlag, Heidelberger Taschenbücher 114 (1973), Kap. 7.3.5 *Die Mehrzielmethode* (pp. 170-191).
4. Deuflhard, P.: Ein Newton-Verfahren bei fastsingulärer Funktionalmatrix zur Lösung von nichtlinearen Randwertaufgaben mit der Mehrzielmethode. Dissertation, Mathematisches Institut der Universität Köln (1972).
5. Deuflhard, P.: A Modified Newton Method for the Solution of Illconditioned Systems of Nonlinear Equations with Application to Multiple Shooting. Numerical Mathematics 22, pp. 289-315, (1974).
6. Schadt, G.H.: Aerodynamic Heating Problems and Their Influence on Earth Orbit Lifting Entry Spacecraft. AIAA Paper No. 68-1126 (Oct. 1968).
7. Dash, M.J.: MDAC Orbiter Temperature Boundaries. S&E-Aero-AT-71-22, NASA-MSFC, Alabama, Nov. 30, 1971.
8. Dickmanns, E.D.: Optimierung von Flugbahnen durch iterative Anwendung des Maximumprinzips. WGLR-Jahrbuch 1967, pp. 272-301 (1968).